

## Characterization of a detector setup for the measurement of the $^{235}\text{U}(n,f)$ cross section relative to n-p scattering up to 500 MeV at the n\_TOF facility at CERN

A. Manna<sup>1,2,\*</sup>, E. Pirovano<sup>3</sup>, N. Colonna<sup>4</sup>, D. Castelluccio<sup>5,2</sup>, P. Console Camprini<sup>5,2</sup>, L. Cosentino<sup>6</sup>, M. Dietz<sup>3</sup>, Q. Ducasse<sup>3</sup>, P. Finocchiaro<sup>6</sup>, C. Le Naour<sup>7</sup>, C. Massimi<sup>1,2</sup>, A. Mengoni<sup>5,2</sup>, R. Nolte<sup>3</sup>, L. Tassan-Got<sup>7,8,9</sup>, N. Terranova<sup>10</sup>, G. Vannini<sup>1,2</sup>, A. Ventura<sup>2</sup>, O. Aberle<sup>8</sup>, V. Alcayne<sup>11</sup>, S. Amaducci<sup>6,12</sup>, J. Andrzejewski<sup>13</sup>, L. Audouin<sup>7</sup>, V. Babiano-Suarez<sup>14</sup>, M. Bacak<sup>8,15,16</sup>, M. Barbagallo<sup>8,4</sup>, S. Bennett<sup>17</sup>, E. Berthoumieux<sup>16</sup>, J. Billowes<sup>17</sup>, D. Bosnar<sup>18</sup>, A. Brown<sup>19</sup>, M. Busso<sup>20,21</sup>, M. Caamaño<sup>22</sup>, L. Caballero-Ontanaya<sup>14</sup>, F. Calviño<sup>23</sup>, M. Calviani<sup>8</sup>, D. Cano-Ott<sup>11</sup>, A. Casanovas<sup>23</sup>, F. Cerutti<sup>8</sup>, E. Chiaveri<sup>8,17</sup>, G. Cortés<sup>23</sup>, M. A. Cortés-Giraldo<sup>24</sup>, S. Cristallo<sup>20,25</sup>, L. A. Damone<sup>4,26</sup>, P. J. Davies<sup>17</sup>, M. Diakaki<sup>9,8</sup>, C. Domingo-Pardo<sup>14</sup>, R. Dressler<sup>27</sup>, E. Dupont<sup>16</sup>, I. Durán<sup>22</sup>, Z. Eleme<sup>28</sup>, B. Fernández-Domínguez<sup>22</sup>, A. Ferrari<sup>8</sup>, K. Göbel<sup>29</sup>, R. Garg<sup>30</sup>, A. Gawlik-Ramięga<sup>13</sup>, S. Gilardoni<sup>8</sup>, I. F. Gonçalves<sup>31</sup>, E. González-Romero<sup>11</sup>, C. Guerrero<sup>24</sup>, F. Gunsing<sup>16</sup>, H. Harada<sup>32</sup>, S. Heinitz<sup>27</sup>, J. Heyse<sup>33</sup>, D. G. Jenkins<sup>19</sup>, A. Junghans<sup>34</sup>, F. Käppeler<sup>†35</sup>, Y. Kadi<sup>8</sup>, A. Kimura<sup>32</sup>, I. Knapová<sup>36</sup>, M. Kokkoris<sup>9</sup>, M. Krčička<sup>36</sup>, D. Kurtulgil<sup>29</sup>, I. Ladarescu<sup>14</sup>, C. Lederer-Woods<sup>30</sup>, H. Leeb<sup>15</sup>, J. Lerendegui-Marco<sup>24</sup>, S. J. Lonsdale<sup>30</sup>, D. Macina<sup>8</sup>, T. Martínez<sup>11</sup>, A. Masi<sup>8</sup>, P. Mastinu<sup>37</sup>, M. Mastromarco<sup>8,4</sup>, E. A. Mauger<sup>27</sup>, A. Mazzone<sup>4,38</sup>, E. Mendoza<sup>11</sup>, V. Michalopoulou<sup>9,8</sup>, P. M. Milazzo<sup>39</sup>, F. Mingrone<sup>8</sup>, J. Moreno-Soto<sup>16</sup>, A. Musumarra<sup>6,40</sup>, A. Negret<sup>41</sup>, F. Ogállar<sup>42</sup>, A. Oprea<sup>41</sup>, N. Patronis<sup>28</sup>, A. Pavlik<sup>43</sup>, J. Perkowski<sup>13</sup>, L. Piersanti<sup>20,25</sup>, C. Petrone<sup>41</sup>, I. Porras<sup>42</sup>, J. Praena<sup>42</sup>, J. M. Quesada<sup>24</sup>, D. Ramos-Doval<sup>7</sup>, T. Rauscher<sup>44,45</sup>, R. Reifarh<sup>29</sup>, D. Rochman<sup>27</sup>, C. Rubbia<sup>8</sup>, M. Sabaté-Gilarte<sup>24,8</sup>, A. Saxena<sup>46</sup>, P. Schillebeeckx<sup>33</sup>, D. Schumann<sup>27</sup>, A. Sekhar<sup>17</sup>, A. G. Smith<sup>17</sup>, N. V. Sosnin<sup>17</sup>, P. Sprung<sup>27</sup>, A. Stamatopoulos<sup>9</sup>, G. Tagliente<sup>4</sup>, J. L. Tain<sup>14</sup>, A. Tarifeño-Saldivia<sup>23</sup>, Th. Thomas<sup>29</sup>, P. Torres-Sánchez<sup>42</sup>, A. Tsinganis<sup>8</sup>, J. Ulrich<sup>27</sup>, S. Urlass<sup>34,8</sup>, S. Valenta<sup>36</sup>, V. Variale<sup>4</sup>, P. Vaz<sup>31</sup>, D. Vescovi<sup>20</sup>, V. Vlachoudis<sup>8</sup>, R. Vlastou<sup>9</sup>, A. Wallner<sup>47</sup>, P. J. Woods<sup>30</sup>, T. Wright<sup>17</sup>, and P. Žugec<sup>18</sup>

<sup>1</sup>Dipartimento di Fisica e Astronomia, Università di Bologna, Italy

<sup>2</sup>Istituto Nazionale di Fisica Nucleare, Sezione di Bologna, Italy

<sup>3</sup>Physikalisch-Technische Bundesanstalt (PTB), Braunschweig, Germany

<sup>4</sup>Istituto Nazionale di Fisica Nucleare, Sezione di Bari, Italy

<sup>5</sup>Agenzia nazionale per le nuove tecnologie (ENEA), Bologna, Italy

<sup>6</sup>INFN Laboratori Nazionali del Sud, Catania, Italy

<sup>7</sup>Institut de Physique Nucléaire, CNRS-IN2P3, Univ. Paris-Sud, Université Paris-Saclay, F-91406 Orsay Cedex, France

<sup>8</sup>European Organization for Nuclear Research (CERN), Switzerland

<sup>9</sup>National Technical University of Athens, Greece

<sup>10</sup>Agenzia nazionale per le nuove tecnologie (ENEA), Frascati, Italy

<sup>11</sup>Centro de Investigaciones Energéticas Medioambientales y Tecnológicas (CIEMAT), Spain

<sup>12</sup>Dipartimento di Fisica e Astronomia, Università di Catania, Italy

<sup>13</sup>University of Lodz, Poland

<sup>14</sup>Instituto de Física Corpuscular, CSIC - Universidad de Valencia, Spain

<sup>15</sup>TU Wien, Atominstitut, Wien, Austria

<sup>16</sup>CEA Irfu, Université Paris-Saclay, F-91191 Gif-sur-Yvette, France

<sup>17</sup>University of Manchester, United Kingdom

<sup>18</sup>Department of Physics, Faculty of Science, University of Zagreb, Zagreb, Croatia

<sup>19</sup>University of York, United Kingdom

<sup>20</sup>Istituto Nazionale di Fisica Nucleare, Sezione di Perugia, Italy

<sup>21</sup>Dipartimento di Fisica e Geologia, Università di Perugia, Italy

<sup>22</sup>University of Santiago de Compostela, Spain

<sup>23</sup>Universitat Politècnica de Catalunya, Spain

<sup>24</sup>Universidad de Sevilla, Spain

<sup>25</sup>Istituto Nazionale di Astrofisica - Osservatorio Astronomico di Teramo, Italy

<sup>26</sup>Dipartimento Interateneo di Fisica, Università degli Studi di Bari, Italy

<sup>27</sup>Paul Scherrer Institut (PSI), Villigen, Switzerland

<sup>28</sup>University of Ioannina, Greece

<sup>29</sup>Goethe University Frankfurt, Germany

<sup>30</sup>School of Physics and Astronomy, University of Edinburgh, United Kingdom

<sup>31</sup>Instituto Superior Técnico, Lisbon, Portugal

- <sup>32</sup>Japan Atomic Energy Agency (JAEA), Tokai-Mura, Japan  
<sup>33</sup>European Commission, Joint Research Centre (JRC), Geel, Belgium  
<sup>34</sup>Helmholtz-Zentrum Dresden-Rossendorf, Germany  
<sup>35</sup>Karlsruhe Institute of Technology, Campus North, IKP, 76021 Karlsruhe, Germany  
<sup>36</sup>Charles University, Prague, Czech Republic  
<sup>37</sup>INFN Laboratori Nazionali di Legnaro, Italy  
<sup>38</sup>Consiglio Nazionale delle Ricerche, Bari, Italy  
<sup>39</sup>Istituto Nazionale di Fisica Nucleare, Sezione di Trieste, Italy  
<sup>40</sup>Dipartimento di Fisica e Astronomia, Università di Catania, Italy  
<sup>41</sup>Horia Hulubei National Institute of Physics and Nuclear Engineering, Romania  
<sup>42</sup>University of Granada, Spain  
<sup>43</sup>University of Vienna, Faculty of Physics, Vienna, Austria  
<sup>44</sup>Department of Physics, University of Basel, Switzerland  
<sup>45</sup>Centre for Astrophysics Research, University of Hertfordshire, United Kingdom  
<sup>46</sup>Bhabha Atomic Research Centre (BARC), India  
<sup>47</sup>Australian National University, Canberra, Australia

### Abstract.

The measurement of the  $^{235}\text{U}(n,f)$  reaction cross section in the neutron energy region 10 MeV to 500 MeV was carried out at the CERN n\_TOF facility. The experimental campaign, completed in 2018, provided precise and accurate data on the fission reaction relative to neutron-proton elastic scattering. A description and characterization of the used setup for the simultaneous measurement of fission fragments and neutron flux is reported here.

## 1 Introduction

The  $^{235}\text{U}(n,f)$  cross section is one of the most important neutron cross-section standards, and therefore it is recognised as a convenient reference for other reaction cross-section measurements at thermal energy and between 0.15 MeV and 200 MeV. Outside these energy ranges, the cross section is either not so well known or not measured yet, as for example above 200 MeV, where evaluations can only rely on theoretical calculations. The  $^{235}\text{U}(n,f)$  reaction plays an important role for fundamental nuclear physics as well as for several applications, ranging from biological dose effect, to nuclear astrophysics and nuclear technology. These considerations led the International Atomic Energy Agency to issue a request for a new absolute measurement of neutron induced fission to improve the situation from 20 MeV to 200 MeV, where only two experimental data sets exist, and to establish a fission cross section standard above 200 MeV [1, 2]. In particular, the request is for fission measurements relative to the neutron-proton elastic scattering, which is considered the primary reference for neutron cross section measurements.

The n\_TOF facility at CERN offers the possibility to study such reaction, thanks to the wide neutron energy spectrum available in the experimental areas, from thermal to 1 GeV. A dedicated measurement campaign has been carried out to provide accurate and precise cross section data of the  $^{235}\text{U}(n,f)$  reaction from 10 MeV to 500 MeV neutron energy. Since the energy region to be investigated is largely unknown, a redundant approach was applied in the adopted experimental setup to reduce the uncertainties involved in the measurement. Therefore, two independent and complementary systems were developed: one focused on the energy region up to about 200 MeV (see ref. [3]), the other with the aim of extending the measurement to energies higher than 200 MeV (discussed here). A detailed

description of the setup and the technical characterization is provided in forthcoming publications [4, 5].

## 2 The experimental setup

The n\_TOF facility is a pulsed neutron source based on the 20 GeV/c proton beam from the CERN Proton Synchrotron accelerator (PS). Protons are accelerated towards a lead spallation target, yielding about 350 neutrons per incident proton. The facility features two beam lines with a white neutron spectrum, and two experimental areas at the nominal distance of 185 m for EAR-1 [6] and 20 m for EAR-2 [7] from the neutron-producing target. The measurement of the  $^{235}\text{U}(n,f)$  cross section was performed in September 2018 in EAR-1, where the neutron spectrum extends up to 1 GeV, and also to profit from the good energy resolution in the high energy region, thanks to the longer flight path.

The experimental apparatus, which involves the efforts of several institutes (INFN <sup>1</sup>, PTB <sup>2</sup> and IPN <sup>3</sup>), consisted of three flux and two fission detectors, thus allowing us to simultaneously record the number of neutrons impinging on the  $^{235}\text{U}$  samples and of fission events, as a function of the neutron energy. Fission events were detected using an ionisation chamber from PTB [8] (PPFC) and a chamber based on Parallel Plate Avalanche Counters (PPACs) developed at IPN [9, 10]. The neutron flux measurement was based on the detection of the recoil protons from the n-p reaction. Two polyethylene targets placed in the neutron beam and three Recoil Proton Telescopes (RPTs) installed at  $\theta = 25^\circ$  and  $\alpha = 20^\circ$  with respect to the neutron beam direction (Fig. 1) were used for this measurement.

<sup>1</sup>Istituto Nazionale di Fisica Nucleare

<sup>2</sup>Physikalisch-Technische Bundesanstalt

<sup>3</sup>Laboratoire de Physique des 2 infinis Irène Joliot-Curie - Institut de Physique Nucléaire d'Orsay

\*e-mail: [almanna@bo.infn.it](mailto:almanna@bo.infn.it)

The three RPTs setup consists of a 3-stage recoil proton telescope (3S-RPT) and two multi-stage recoil proton telescopes (MS-RPTs). The basic concept is to select only the events in coincidence between the layers and apply the  $\Delta E - E$  method for particle identification ( $\Delta E - E \propto z^2 M$  - where  $z$  and  $M$  are the charge and the mass of the particle, respectively). It is a prerequisite for discriminating protons from other charged particles which are produced by neutron reactions with the carbon present in the polyethylene target.

The PPFC and 3S-RPT are illustrated and described in detail in ref. [3]. Here, a focus on the setup realized to study the cross section up to 500 MeV, achieved by combining PPAC and MS-RPTs data, is provided.

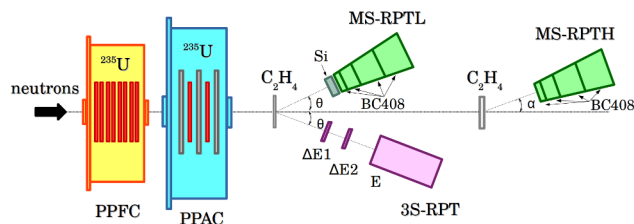


**Figure 1.** Scheme of the setup used at n\_TOF for the measurement of the  $^{235}\text{U}(n,f)$  cross section. Fission events were measured with a Parallel Plate Ionization Chamber (PPFC) and a set of Parallel Plate Avalanche Counters (PPACs). Recoil protons were detected and identified in three different telescopes, placed at a small angle outside the neutron beam.

### 3 Multi-Stage Recoil Proton Telescope

The two MS-RPTs were designed in order to be as compact as possible. A sketch of the structure of one MS-RPT is shown in Fig. 2. The two MS-RPTs work in two different energy ranges with an overlapping region. The low energy detector (MS-RPTL) is optimized for reaction of neutrons with energy from 10 MeV to 150 MeV; the high energy telescope (MS-RPTH) works above 100 MeV. Both MS-RPTs consist of a trapezoidal structure pointing to the radiator polyethylene sample. They are composed of four independent BC408 plastic scintillators [11] with increasing thickness of 0.5 cm, 3.0 cm, 6.0 cm and 6.0 cm. The last three slabs are read out independently through the coupling, at the center of a side face, with a 1" Hamamatsu R1924A Photomultiplier tube (PMT). The light collection of the first scintillator has a sizable dependence on the impact point of the particle, due to its reduced thickness, therefore it is coupled with two light-guides each with a PMT on opposite sides of the scintillator. The MS-RPTL has two silicon detectors placed in front of the first thin scintillator. The silicon detectors MSX09-300 [12], 300  $\mu\text{m}$  thick, were installed in a dedicated holder, 7 mm apart from each other with a 4  $\mu\text{m}$  thick aluminum foil placed on the entrance and exit windows. Thanks to the coincidence condition between the silicon detectors, the minimum detectable neutron energy is 10 MeV, while a minimum of 40 MeV is obtained by the coincidence of the first two plastic scintillators.

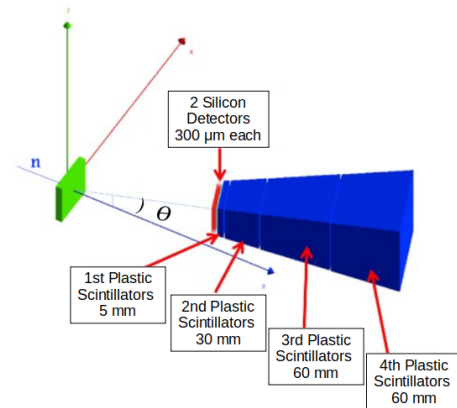


**Figure 2.** A geometrical drawing of the MS-RPTL: the two silicon detectors followed by the four plastic scintillators.

As already mentioned, the analysis approach adopted is based on the identification of events in coincidence between the layers of the MS-RPT and the identification of different particles by means of the  $\Delta E - E$  method. Extensive simulations with neutrons impinging on a realistic setup, composed of the polyethylene or carbon sample and the MS-RPTs, were performed [13] to evaluate the detection efficiency.

Figure 3 shows an example of the  $\Delta E - E$  matrix produced by Monte Carlo simulations taking into account the events produced by neutrons with energy of  $(74.8 \pm 2.2)$  MeV. The plots 3(a) and 3(b) show the charge particles (protons and deuterons) produced in the  $\text{C}_2\text{H}_4$  and the C target, respectively which are stopped in the second plastic scintillator. The different types of nuclear reactions involving carbon and hydrogen are clearly separated (Fig. 3(c)):

- in the case of n+H reaction, only protons are present in the  $\Delta E$ -E matrix and their energy is distributed around the corresponding kinematic locus (defined by  $E_p = E_n \cos^2\theta$ );
- in the case of n+C reaction, in addition to protons other particles are present. The energy distribution of emitted particles has a lower mean value and the kinematics of the nuclear reaction does not produce a peaked distribution in energy, therefore the events are distributed throughout the whole hyperbola.

The particle selection and the subtraction of events arising from reactions with carbon from the total events recorded with polyethylene isolates the contribution of n-p recoiled protons. Applying the same analysis conditions both in the experimental and in the simulated data, it is possible to extract the neutron flux.

### 4 Parallel Plate Avalanche Counters

The PPAC is a type of gas detector that operates in avalanche regime, which is defined by a combination of gas pressure and electric field. The detector design of each PPAC consists of 3 parallel plate electrodes: a central anode surrounded by two cathodes. The electrodes, with an area of  $20 \times 20 \text{ cm}^2$ , are made of 1.7  $\mu\text{m}$  thick mylar foils,

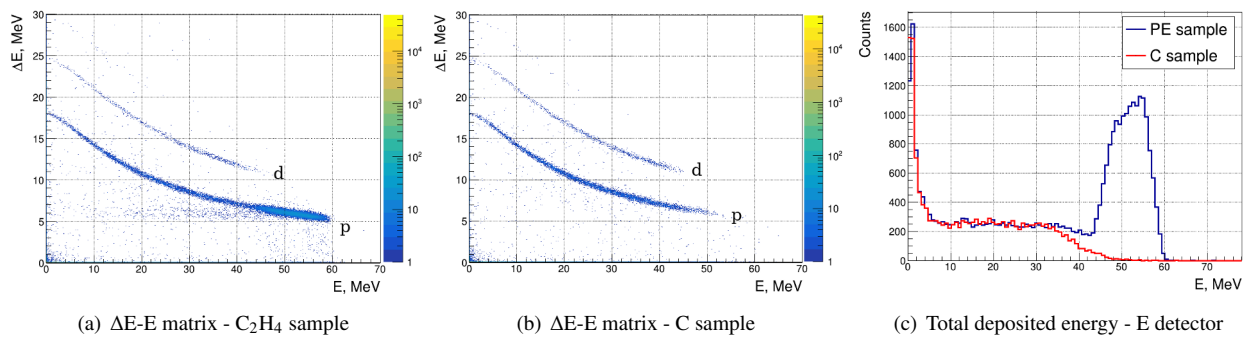


**Figure 3.** Figures 3(a) and 3(b) show the  $\Delta E - E$  matrices produced by the Monte Carlo simulation – choosing the events of neutrons with energy of  $(74.8 \pm 2.2)$  MeV hitting the  $C_2H_4$  and the C sample, respectively. The one-dimensional histogram 3(c) shows the total deposited energy in the  $E$  detector for the  $C_2H_4$  sample in blue and the C sample in red.

coated with gold, 700 nm thick, to make them conductive. For the anode the coating is uniform and double sided, whereas for the cathodes the coating is divided into 2 mm wide strips. The golden strips have a width of 1.9 mm and are separated by 0.1 mm.

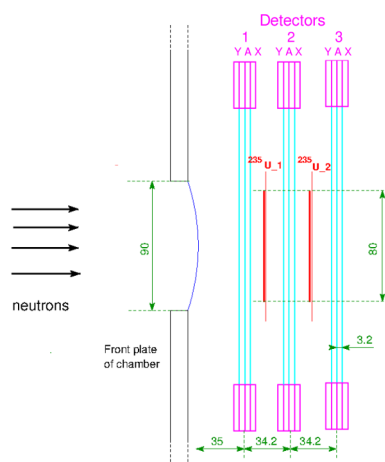


**Figure 4.** Schematic view of the experimental setup with three PPACs and two  $^{235}U$  samples. All dimensions are expressed in mm.

The design of this PPAC allows one to detect in coincidence the two fission fragments emitted in the fission process. In this way, a high signal-to-background ratio is obtained. In order to apply the coincidence technique, a detection cell is made of a uranium sample surrounded by two PPACs, as sketched in Fig. 4. As a consequence, the backing supporting the deposited layer of the isotope being measured has to be thin enough to allow the emitted fragment to be detected. The two samples used in the present measurement consisted of a deposit of  $^{235}U$  with 8 cm diameter. The impurities consist of other uranium isotopes, analysed by mass spectrometry, as follows:  $^{234}U/^{235}U=0.007472(15)$ ,  $^{236}U/^{235}U=0.002696(5)$ ,  $^{238}U/^{235}U=0.06283(6)$ . The second sample was characterized by alpha counting. The uniformity was measured by scanning at short distance the activity with a collimated silicon detector with a 3.5 mm

step (in x and y), while the total amount was measured by long distance alpha counting, showing an averaged  $^{235}U$  density of  $280 \mu\text{g}/\text{cm}^2$  with an accuracy better than 1% [4].

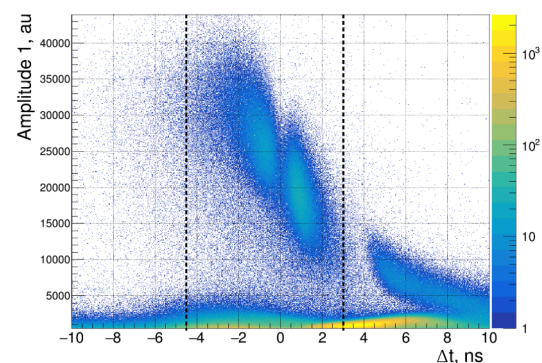


**Figure 5.** Correlation between amplitude on detector 1 with the time difference ( $\Delta t$ ) between detector 2 and 1.

An example of the good discrimination of fission and background events is shown in Fig. 5. The plot shows the amplitude of the events in the first anode, in coincidence with the detector 1 and 2 surrounding the first target, versus the difference in time between the events in the two detectors. The spots at  $\Delta t \approx 0$  correspond to the fission fragments emitted by the first  $^{235}U$  target. The two bumps indicate the asymmetric nature of the fission process: the spot at higher amplitude is due to the case where detector 1 is hit by the light fragment and detector 2 by the heavy fragment; the lowest one is for the reverse case. The signals at a time difference  $\Delta t$  of about 7 ns are due to the fragments emitted by the second  $^{235}U$  target. A time selection of about  $\pm 4$  ns allows one to select the fragments emitted by the first target only. In addition, the amplitude of the events produced by fission fragments is clearly separated from the low-amplitude background events (e.g.  $\alpha$  activity events). This technique allows to detect only fission fragments emitted in a forward cone with an opening angle of at most  $60^\circ$ . Therefore, a detailed study of the efficiency as a function of the energy, including both the angular dis-

tribution of the fission fragments and the relativistic boost, was carried out (for more details see ref. [4]).

## 5 Conclusion

The neutron-induced fission cross-section of  $^{235}\text{U}$  as a function of the neutron kinetic energy was measured at the neutron time-of-flight facility n\_TOF at CERN. The fission events detected by the PPAC detector and the neutron flux measured by means of the two MS-RPTs allowed us to derive the cross section (related to the n-p scattering) in the neutron energy range between 10 MeV and 500 MeV.

The redundant approach enable a comparison between different detectors and better quantify and reduce the systematic uncertainties. Even more, the agreement between the detection system used in the low energy region (PPFC and 3S-RPT) and the one that aims to extend the cross section results above 200 MeV (PPAC and MS-RPTs) is fundamental for the validation and demonstration of the reliability of experimental results in the higher energy region.

The experimental setup described here has been validated to extend the measurement of the neutron induced fission cross section on  $^{235}\text{U}$  up to 500 MeV.

## Acknowledgements

In line with the principles that apply to scientific publishing and the CERN policy in matters of scientific publications, the n\_TOF Collaboration recognises the work of

V. Furman and Y. Kopatch (JINR, Russia), who have contributed to the experiment used to obtain the results described in this paper.

## References

- [1] A. D. Carlson et al., Nucl. Data Sheets **148**, 143-188 (2018)
- [2] E. Dupont et al., EPJ Web of Conferences **239**, 15005 (2020)
- [3] E. Pirovano et al. (the n\_TOF Collaboration), Proceeding of the International Conference on Nuclear Data for Science and Technology, (2022)
- [4] A. Manna et al., in preparation, (2022).
- [5] E. Pirovano et al., in preparation (2022).
- [6] C. Guerrero et al. (the n\_TOF Collaboration), Eur. Phys. J. A **49**, (2013)
- [7] C. Weiss et al. (the n\_TOF Collaboration), NIM A **799**, 90 (2015)
- [8] D.B. Gayther et al., Metrologia **27**, 221 (1990)
- [9] C. Paradela et al. (the n\_TOF Collaboration), Phys. Rev. C **82**, 034601 (2010)
- [10] D. Tarrío et al. (the n\_TOF Collaboration), Phys. Rev. C **83**, 044620 (2011)
- [11] <https://www.crystals.saint-gobain.com/products/bc-408-bc-412-bc-416>.
- [12] <http://www.micronsemiconductor.co.uk/>.
- [13] N. Terranova et al. (the n\_TOF collaboration), EPJ Web of Conferences **239**, 01024 (2020)